The *Candida albicans* Cdk8-dependent phosphoproteome reveals repression of hyphal growth through a Flo8-dependent pathway

Jeffrey M. Hollomon[#a], Zhongle Liu[# a], Scott F. Rusin[b], Nicole P. Jenkins[b], Allia K. Smith[a], Katja Koeppen[a], Arminja N. Kettenbach[b], Lawrence C. Myers[b]*, and Deborah A. Hogan[a]*

[a]Department of Microbiology and Immunology, Geisel School of Medicine at Dartmouth, Hanover, NH 03755
[b]Department of Biochemistry and Cell Biology, Geisel School of Medicine at Dartmouth, Hanover, NH 03755

[#]Both authors contributed equally to this work.

*To whom correspondence should be addressed:

Deborah A. Hogan

Geisel School of Medicine at Dartmouth

Rm 208 Vail Building, Hanover, NH 03755

E-mail: dhogan@dartmouth.edu

Tel: (603) 650-1252

Lawrence Myers

Geisel School of Medicine at Dartmouth

Vail Building, Hanover, NH 03755

E-mail: lawrence.c.myers@dartmouth.edu

Abstract:

Ssn3, also known as Cdk8, is a member of the four protein Cdk8 submodule within the multi-subunit Mediator complex involved in the co-regulation of transcription. In *Candida albicans*, the loss of Ssn3 kinase activity affects multiple phenotypes including cellular morphology, metabolism, nutrient acquisition, immune cell interactions, and drug resistance. In these studies, we generated a strain in which Ssn3 was replaced with a functional variant of Ssn3 that can be rapidly and selectively inhibited by the ATP analog 3-MB-PP1. Consistent with *ssn3* null mutant and kinase dead phenotypes, inhibition of Ssn3 kinase activity promoted hypha formation. Furthermore, the increased expression of hypha-specific genes was the strongest transcriptional signal upon inhibition of Ssn3 in transcriptomics analyses. Rapid inactivation of Ssn3 was used for phosphoproteomic studies performed to identify Ssn3 kinase substrates associated with filamentation potential. Both previously validated and novel Ssn3 targets were identified. Protein phosphorylation sites that were reduced specifically upon Ssn3 inhibition included two sites in Flo8 which is a transcription factor known to positively regulate *C. albicans* morphology. Mutation of the two Flo8 phosphosites (threonine 589 and serine 620) was sufficient to increase Flo8-HA levels and Flo8 dependent activity, suggesting that Ssn3 kinase activity negatively regulates Flo8. Previous work has also shown that loss of Ssn3 activity leads to increased alkalinization of medium with amino acids. Here, we show that *FLO8* and *STP2*, a transcription factor involved in amino acid utilization, are required for *ssn3*Δ/Δ phenotype, but that loss of the Ssn3 phosphosites identified in Flo8 was not sufficient to phenocopy the *ssn3*Δ/Δ mutant. These data highlight the spectrum of processes

affected by the modulation of Ssn3 activity and underscore the importance of considering Ssn3 function in the control of transcription factor activities.

Introduction

One of the important roles of the Mediator transcriptional co-regulatory complex is to link the activity of promoter-bound transcriptional factors to the basal transcription machinery. The Cdk8 sub-module of Mediator plays important roles in modulating the activity of Mediator itself as well as the activity of transcription factors, among other proteins. In *Candida albicans*, like in other eukaryotes, the Cdk8 module consists of four subunits: the catalytic subunit Ssn3 (Cdk8), Ssn8 (CycC), Med12 (Srb8), and Med13 (Srb9). Ssn3, the catalytic component of the Cdk8 module, is a cyclin-dependent like kinase and its activity depends on the cyclin-like protein Ssn8. Across eukaryotic species, the Cdk8 kinase has been shown to be particularly important for regulation during metabolism and morphpology (1, 2). In mammals, for example, glycolysis, lipogenesis and immune responses are influenced by Cdk8 phosphorylation of specific regulators (3-5). In *S. cerevisiae*, Ssn3(Cdk8) has been well-studied for its roles in metabolism (6, 7) and its negative regulation of pseudohyphal growth through Ste12 (8) and Phd1 (9, 10). The Cdk8 module is of particular interest for its role in transitions between growth conditions and during development as cells need to rapidly make coordinated changes to the abundances and activities of cellular regulators.

In *C. albicans*, null mutations in either *SSN3* or *SSN8* result in interrelated, pleiotropic phenotypes. *SSN3* null mutants had increased induction of drug resistance elements (11) and increased resistance to the effects of bacterially-produced metabolic inhibitors (12). The *ssn3*Δ/Δ leads to a hyperwrinkled colony morphology, increased respiratory metabolism and amino acid utilization (12), and fraction of Ras1 in its active GTP-bound state (13). Mutation of *SSN3* was found to unmask an alternative

filamentation pathway in macrophages (14). Recent work by Lu and colleagues (15) found that changes in Ssn3 activity in response to CO_2, mediated by the Ptc2 phosphatase, led to decreased Ssn3 phosphorylation and decreased inhibition of Ume6, a positive regulator of hyphal growth.

Here, we utilize analog-sensitive variants of *C. albicans* Ssn3, as has been performed in *S. cerevisiae* and in human cells, (3, 16), to study the immediate effects of inhibition of Cdk8 kinase activity on *C. albicans*. Under conditions that do not promote hyphal growth in wild-type strains, Ssn3 inhibition led to the formation of hyphae. We used these conditions to elucidate the *C. albicans* Cdk8 regulon as it related to the control of morphology using phosphoproteomic and transcriptomic analysis of cells shortly after Ssn3 inhibition. Flo8, a transcription factor that positively regulates hyphal growth (17, 18), was identified in the phosphoproteomics analysis as a candidate for Ssn3 regulation, and transcriptomics data showed alterations in hypha-specific genes known to be regulated by Flo8. Deletion of Ssn3-phosphosites in Flo8 was sufficient to affect protein levels and morphology. Additional assays suggest that Flo8 plays major roles in Ssn3-regulated control of metabolism. The data in this manuscript indicate the spectrum of proteins that are altered, directly or indirectly, by Ssn3 kinase activity as cells respond to changing environments. While these studies focus on Flo8, our data show that other transcription factors, including Efg1 and Eed1 are also likely Ssn3 targets and thus the tools and insights presented here may aid in the study of diverse proteins involved in morphology, virulence and drug resistance.

RESULTS:

3-MB-PP1 inhibits analog-sensitive Ssn3

To investigate the direct targets of the *C. albicans* Ssn3 kinase, we sought to develop a strain in which Ssn3 kinase activity could be rapidly inhibited using approaches that have been successfully applied in *S. cerevisiae* (16). Based on the alignment of the *C. albicans* and S*. cerevisiae* Ssn3 orthologs, we predicted a phenylalanine to glycine substitution at position 257 would yield a variant that retained the functions of the wild-type kinase, while still being able to be specifically inhibited by the ATP analog 3-MB-PP1 (19). The $Ssn3^{F257G}$ was constructed and is henceforth referred to as the analog-sensitive variant, $Ssn3^{AS}$.

We first assessed the inhibition of $Ssn3^{AS}$ by 3-MB-PP1 with an *in vitro* kinase assay using purified Mediator complex containing the Cdk8 module. $Ssn3^{WT}$ or $Ssn3^{AS}$ were expressed in a background that contained a His-FLAG-tagged derivative of Ssn8 for purification. The activity of $Ssn3^{WT}$ or $Ssn3^{AS}$ was assessed using ^{32}P *in vitro* kinase assays (20) in which phosphorylation of recombinantly produced C-terminal domain (CTD) of RNA Pol II, an Ssn3 substrate, was monitored. The $Ssn3^{WT}$ and $Ssn3^{AS}$ kinases had equal CTD phosphorylation activity in the absence of inhibitor (**Fig. 1**). The $Ssn3^{AS}$ kinase activity was inhibited by 3-MB-PP1 in a dose-responsive fashion, while addition of this compound had no effect on the $Ssn3^{WT}$ kinase activity (**Fig. 1**). A concentration of 2.7 μM 3-MB-PP1 inhibited ~85% of the $Ssn3^{AS}$ activity and 24 μM virtually eliminated the activity.

In order to determine if Ssn3 kinase activity could be inhibited *in vivo,* we engineered a derivative of *C. albicans* SC5314 in which both alleles of *SSN3* had been

94 replaced by *ssn3*^{AS}. We also constructed a strain with two copies of the *ssn3-D325A*
95 allele, which encodes a non-functional, or kinase dead, Ssn3 variant (21) due to mutation
96 of a key aspartate in the catalytic site. This kinase-dead variant is referred to here as
97 *ssn3*^{KD}. We have previously shown that, under certain growth conditions, *ssn3*Δ/Δ
98 mutants form hyperwrinkled colonies compared to the SC5314 wild type (WT) (12), a
99 phenotype associated with increased hyphal growth. Thus, we asked if the Ssn3^{AS}-
100 expressing strain had a hyperfilamentous phenotype specifically in the presence of 3-MB-
101 PP1 and not in its absence. To quantify hypha formation differences in WT, *ssn3*^{AS}, and
102 *ssn3*^{KD} strains, we identified conditions which revealed differences in the propensity for
103 hypha formation among strains. Thus, we grew cells in YNB containing amino acids and
104 N-acetyl-glucosamine (GlcNAc), both of which are inducers of hyphal growth (YNBAG),
105 but incubated cultures at 30˚C, a temperature lower than that generally used to induce
106 robust hyphal growth. All cultures were amended with either 3-MB-PP1 or the vehicle
107 DMSO. The morphology of the WT was almost entirely yeast and pseudohyphae, and the
108 relative fractions of these morphologies were unaffected by 5 μM 3-MB-PP1 (**Fig. 2A**).
109 While the *ssn3*^{AS} cells were similar to the WT in vehicle control cultures, the addition of
110 3-MB-PP1 to *ssn3*^{AS} cultures caused a significant increase in the number of hyphae (**Fig.**
111 **2**). The increase in the fraction of cells in the hyphal morphology in 3-MB-PP1 treated
112 *ssn3*^{AS} was concomitant with a significant decrease in the fraction of cells present as
113 yeast (**Fig. 2A**). The *ssn3*^{KD} strain formed significantly more hyphae than the WT and
114 *ssn3*^{AS} strains in control conditions, and the fraction of cells as hyphae was unaffected by
115 the addition of 3-MB-PP1 (**Fig. 2A-B**). Together, these data indicated that 5 μM 3-MB-

PP1 inhibits Ssn3^{AS} *in vivo* and that the ATP analog has no discernable effects on the morphology of WT or *ssn3^{KD}* strains.

Transcriptomics analyses reveal inhibition of Cdk8 by 3-MB-PP1 leads to the induction of hypha-specific genes

To further explore the effects of Ssn3 inhibition on the regulation of hypha formation (12) and on transcription more broadly, we examined the transcriptomes of *ssn3^{AS}* and WT strains grown with 3-MB-PP1 or DMSO vehicle. The WT strain was included in this experiment to assess off-target effects of 3-MB-PP1. Cells from stationary phase cultures were inoculated into the same medium used for morphology assessment, YNBAG, with either 5 μM 3-MB-PP1 or an equivalent volume of DMSO. Three replicate cultures for each strain-treatment combination were incubated for 60 min at 30°C prior to RNA harvest and sequencing as described in the methods. In the *ssn3^{AS}* strain, we found that 249 genes were significantly up regulated upon treatment with 3-MB-PP1 by 2- to 49-fold ($p<0.05$ FDR); transcripts for 33 genes were significantly lower by more than 2-fold with treatment (**Table S2**). Fewer genes were affected by 3-MB-PP1 in the WT with 157 and 4 genes significantly increased and decreased, respectively; the magnitudes of the changes were also smaller (2- to 6-fold) (**Table S2**). The greater number of transcripts at higher levels upon inhibition of Ssn3 is consistent with the Cdk8 module being a predominantly negative regulator of transcription factors (3) or the transcriptional re-initiation or "pausing" of RNA polymerase II (reviewed in (22)). We found seventy-seven transcripts that exhibited a significant fold increase (>2-fold) in both the comparison of the *ssn3^{AS}* strain treated with 3-MB-PP1 to its treatment with DMSO, and the comparison of

3-MB-PP1-treated *ssn3*^{AS} strain to 3-MB-PP1-treated WT (**Fig. 3** with gene expression shown in log2-transformed counts per million). Consistent with phenotypic analysis of the effects of Ssn3 inhibition on morphology, transcripts encoding *ECE1* and *HWP1* were two of the most highly induced by Ssn3 inhibition in the AS strain (46- and 22-fold higher, respectively). Other transcripts differentially-increased upon Ssn3 inhibition included genes associated with hyphal morphology, such as *ALS1*, *ALS3*, *IHD1*, *RBT1*, *HYR1*, and *HGC1* (14, 23). Consistent with the previous finding that Ssn3 represses induction of Mrr1 controlled genes, *MDR1* was significantly induced with Ssn3 inhibition (11).

Specific inhibition of Ssn3 affects the phosphoproteome during the induction of hyphal growth

To identify direct phosphorylation targets of Ssn3 that led to changes in phenotype and the transcriptome, we used mass spectrometry to quantitatively analyze the phosphoproteomes of the *ssn3*^{AS} strain compared to the WT after 3-MB-PP1 treatment. We grew *ssn3*^{AS} and WT cells to stationary phase, then incubated culture aliquots with 5 μM 3-MB-PP1 for five minutes to allow for drug entry into the cell. We then added concentrated, fresh, pre-warmed YNBAG medium to reproduce the conditions that induce hyphal growth in strains with low Ssn3 activity but not in the WT. Cultures were incubated for an additional 15 min at 30°C with shaking followed by rapid harvest in order to minimize secondary effects of Ssn3 inhibition. Cells were lysed under liquid nitrogen by grinding. We conducted three replicate experiments across three different days, each from an independent overnight culture to increase the robustness of our experimental design.

To reveal the direct targets of Ssn3, we focused on phosphosites that became less abundant in the presence of 3-MB-PP1 in the *ssn3*^{AS} strain, but not the WT (**Table 1** and **Table S3** for complete dataset). We found that 977 phosphopeptides mapping to 552 proteins were depleted in *ssn3*^{AS} compared to WT, setting a 2-fold cutoff in addition to the P<0.05 test for significance (**Table 1**). Within this group of depleted phosphosites, 82.7% were serines, 15.8% were threonines, and 1.5% were tyrosines. These proportions are very similar to those we observed with a quantification of the whole *C. albicans* phosphoproteome (20), with a slight increase in the number of phosphoserines and a concomitant decrease in the number of phosphothreonines. Although promiscuous, Cdks have been described as proline-directed kinases, and consistent with this, 293 phosphopeptides contained prolines in the position adjacent to C-terminal side of the phosphoresidue, referred to as the Proline Motif (**Table 1**) (24). Fewer phosphosites were found within common RXS/T motifs, in which arginine is in the -2 position relative to the phosphoserine or phosphothreonine, (25). We observed that 264 phosphopeptides (202 proteins) were significantly enriched upon Ssn3 inhibition. This increase in phosphorylation likely represents indirect or secondary effects of Ssn3 inhibition.

We found 218 proteins that contained phosphosites covered by 2 or more depleted phosphopeptides (a consideration taken to increase stringency) in the *ssn3*^{AS} strain compared to WT, and of these 218 proteins, 40 were annotated as having known or predicted nuclear localization in UniProt **(Fig. 4)**(26). Among these, we found that Ssn3^{AS} inhibition led to depletion of phosphopeptides from Med4, with phosphorylated S21 and S33, which is notable as these have previously been identified as target sites for the *C. albicans* Ssn3 kinase (20). We also observed depletion of specific phosphosites (T589

and S620) in Flo8, a regulator of filamentous growth in both *C. albicans* and *S. cerevisiae* (17, 18, 27), and both T589 and S620 were found within the aforementioned proline motif (**Table 1**). Our transcriptomic data showed that *FLO8* levels were unchanged by either Cdk8 inhibition or 3-MB-PP1 addition (**Table S2**). While we focus on Flo8 in the studies presented here, it is worth noting that other hyphal growth associated transcription factors, such as Efg1 were found among the proteins with phosphosites that were at lower abundance with Ssn3 inhibition as discussed below.

Flo8 is required for Ssn3-dependent hyperfilamentation and hypha-specific gene expression.

To determine whether there was a genetic interaction between *SSN3* and *FLO8* that accompanied the phosphoproteomic data above, we investigated the phenotype of single and double null mutants of these two genes. We previously reported that an *ssn3* null mutant forms wrinkled colonies in the presence of a metabolic inhibitor, pyocyanin, while the WT does not (12). While both the *ssn3* null strain and the WT formed smooth colonies on YNBA agar at 30˚C (which is the same as YNBAG used above but without GlcNAc), only the ssn3Δ/Δ formed wrinkled colonies at 37˚C. Similarly, the *ssn3*Δ/Δ strain, but not the WT, formed wrinkled colonies on solid YNBA medium with 110 mM added glucose (**Fig. 5A**). This wrinkled colony phenotype of the *ssn3*Δ/Δ mutant under the above conditions was abolished upon deletion of *FLO8* (*ssn3*Δ/Δ*flo8*Δ/Δ) (**Fig. 5A**). The *flo8*Δ/Δ mutant formed smooth colonies, like the WT, under all conditions. In liquid medium, we observed a similar epistatic relationship between *FLO8* and *SSN3*. Only the *ssn3*Δ/Δ strain, and not the WT, formed hyphae and the hyperfilamentation phenotype in *ssn3*Δ/Δ

was dependent on *FLO8* (**Fig. 5B**). Expression levels of hypha-specific transcripts that were induced upon inhibition of Ssn3^{AS} (**Fig. 3**) were significantly higher in the *ssn3*Δ/Δ background compared to the WT, but not in the ssn3Δ/Δ*flo8*Δ/Δ background (**Fig. 5C**). In **Fig. 6**, we demonstrate the ability to complement the filamentation defects of the *flo8*Δ/Δ and *ssn3*Δ/Δ*flo8*Δ/Δ with the native *FLO8* allele, and this result is described in more detail below.

We also found that the *ssn3*Δ/Δ strain was hyperfilamentous in comparison to the WT in embedded conditions, and that deletion of *FLO8* in the *ssn3*Δ/Δ background was able to suppress this phenomenon (**Fig. 5D**). Cao et al. (17) reported that *FLO8* was necessary for embedded filamentation and we reproduced this result (**Fig. 5D**). To determine whether *FLO8* is also required for embedded hyphal growth in *efg1*Δ/Δ, another strain that is hyperfilamentous under embedded conditions (28, 29), we generated a *flo8* and *efg1* null double mutant. We found that *FLO8* disruption suppressed embedded filamentation in the *efg1*Δ/Δ background (**Fig. S1A**).

Loss of putative Ssn3-phosphosites in Flo8 leads to increased filamentation

To study the effects of Ssn3 activity on Flo8 protein, we complemented the *ssn3*Δ/Δ*flo8*Δ/Δ mutant with an allele that encodes a 3XHA-Flo8. This allele restored the hyperfilamentous *ssn3*Δ/Δ phenotype to the *ssn3*Δ/Δ*flo8*Δ strain (**Fig. 6A**). To further explore the effects of Flo8 phosphorylation by Ssn3, we generated an allele in which both T589 and S620, the sites identified in the phosphoproteomics analysis of the Ssn3^{AS} bearing strain, were mutated to alanines (a phospho-incompetent residue) or glutamic acid (which also abolishes phosphorylation, but sometimes can serve as a

229 phosphomimetic) to determine whether these residues play roles in the morphological
230 phenotype of Cdk8 inhibition. Neither the WT or *flo8Δ/Δ* strain gave a wrinkled colony
231 morphology on either medium (**Fig. 6A**) and, as expected, complementation of the *flo8*Δ/Δ
232 with epitope tagged Flo8 did not change colony morphology. However, complementing
233 the *flo8Δ/Δ* strain with either *flo8*$^{T589A,\ S620A}$ or *flo8*$^{T589E,\ S620E}$ led to a wrinkled colony
234 phenotype in the presence 110 mM glucose, suggesting that the phosphorylation of Flo8,
235 potentially via Ssn3, represses Flo8 activity and that the absence of these sites releases
236 that repression (**Fig. 6A**). Consistent with the increased wrinkled colony phenotype in the
237 *flo8*Δ/Δ strains with *flo8*$^{T589A,\ S630A}$ or *flo8*$^{T589E,\ S620E}$ relative to the strain with unmutated
238 *FLO8*, both Flo8 variants also led to increased hyphal development in YNBAG (**Fig. 6B**).
239 Because both *flo8*$^{T589A,\ S620A}$ and *flo8*$^{T589E,\ S620E}$ alleles conferred increased filamentation
240 phenotypes consistent with high Flo8 activity in *flo8*Δ/Δ and *ssn3*Δ/Δ*flo8*Δ/Δ strains we
241 concluded that the Flo8^{T589E,S620E} variant was not acting as a phosphomimetic, but rather
242 both had phenotypes consistent with decreased negative regulation. To quantitatively
243 assess the differences in activity of the morphology program attributed to the loss of
244 putative Ssn3 phosphorylation sites, levels of hypha-associated transcripts were
245 measured in the *flo8*Δ/Δ strains with either HA-tagged *FLO8* or *flo8*$^{T589A,\ S620A}$ (**Fig. 6C**).
246 We found significantly increased expression levels of several core filamentation response
247 genes in the strain with *flo8*$^{T589A,\ S620A}$ versus that with *FLO8*.

248 In multiple instances, phosphorylation by Ssn3 leads to decreased levels of
249 transcription factors (6, 8, 15). Thus, we tested the hypothesis that Flo8-HA^{T589A,S620A} and
250 Flo8-HA^{T589E,S620E} were present at higher levels than Flo8-HA. We found that indeed the
251 two variants were present at higher relative levels compared to Flo8-HA in an *SSN3* wild-

type background. Furthermore, Flo8-HA levels were higher in an *ssn3*Δ/Δ strain than in the *SSN3/SSN3* (+/+) strain which no significant differences in levels for the native and variant proteins. In order to address the slight difference in migration of Flo8-HA in the Δ/Δ strain backgrounds (**Fig. 6D**), we analyzed the migration of FLO8-HA in backgrounds with active Ssn3 (WT and *ssn3*^{AS}) and strains lacking Ssn3 activity (*ssn3*Δ/Δ and *ssn3*^{KD}) (**Fig. 6E**). We confirmed that in the absence of Ssn3 activity, Flo8 migration was slightly faster suggesting that other post-translational modifications (e.g. additional phosphorylations) are controlled by Ssn3. It is worth noting that one other Flo8 phosphosite was identified, but it did not reach the significance cutoff.

Ssn3 metabolic hyperalkalinization phenotype depends on Flo8

Previous work has shown that the *C. albicans ssn3*Δ/Δ mutant differed from the WT in glycolysis and the utilization of amino acids (12). By analyzing the differentially abundant transcripts upon inhibition of Ssn3, we identified statistical enrichment of genes in KEGG pathways involved in amino acid metabolism and glycolysis (**Table S4**). These pathways could represent a potential connection between the *ssn3*Δ/Δ hyperalkalinization phenotype which is dependent on amino acid catabolism and concomitant release of ammonia (12). When grown on amino acid-containing YNBA, alkalinization of the agar medium, evident by the color change of the pH indicator, by the *ssn3*Δ/Δ mutant was less sensitive than WT to inhibition caused by increasing glucose concentrations which leads to production of acidic fermentation products. The previously observed alkalinization of the medium by the *ssn3Δ/Δ* strain (12) is consistent with increased alkalinization due to amino acid catabolism. To determine whether Ssn3 influences medium alkalinization

through this mechanism, we constructed a *ssn3*Δ/Δ*stp2*Δ/Δ double mutant. Stp2 is a transcription factor involved in ammonia release from amino acid catabolism and is a downstream component of the SPS system (30). *STP2* disruption resulted in a defect in alkalinization at 5.5 mM glucose compared to WT and suppressed the hyperalkalinization phenotype of the *ssn3*Δ/Δ strain at both 27.5 mM and 110 mM glucose (**Fig. 7A**). This is consistent with a model in which the SPS amino acid sensing pathway and subsequent generation of ammonium through amino acid catabolism are primarily responsible for the hyperalkalinization phenotype of *SSN3* inactivation.

FLO8 was required for the hyperalkalinization phenotype of the *ssn3*Δ/Δ strain and the phenotype was complemented by reintroducing *FLO8* (**Fig. 7B**), a result that paralleled the Flo8 requirement for hyperfilamentation in the *ssn3*Δ/Δ strain. In contrast, the *flo8*Δ/Δ strain did not differ from the WT in its effects on medium pH, suggesting that Flo8 effects on medium pH were associated with decreased Ssn3 activity (**Fig. 7A**). While complementation of the *ssn3*Δ/Δ*flo8*Δ/Δ double mutant with the wild-type *FLO8* allele restored the metabolic phenotypes, complementation with either $flo8^{T589A,S620A}$ or $flo8^{T589E,S620E}$ did not exacerbate the phenotype further. Similarly, complementation of the *flo8*Δ/Δ single mutant with the Flo8 variants did not generate changes in alkalinization compared to complementation with the native allele suggesting that Ssn3 effects on metabolism may require other factors directly or indirectly regulated by Ssn3.

Discussion:

In this work, we used strains with an analog-sensitive *ssn3* allele, a catalytically inactive *ssn3* allele and null mutants to assess how Ssn3 and its kinase activity regulate

hyphal growth and metabolism. We identified 754 proteins with significant, differential phosphorylation (>2-fold, $p<0.05$) upon inhibition of Ssn3 during the yeast to hypha transition and they included Med4, a known Ssn3 substrate, and Flo8, a known regulator of hyphal growth (17, 18). We show that in a variety of conditions, the loss or decrease in Ssn3 activity leads to increased hypha formation and hypha-specific gene expression and that both phenotypes were dependent on Flo8. Through mutagenesis of the two Ssn3 phosphorylation sites (T589 and S620), we found that mutation of these sites was sufficient to increase filamentation and hypha-associated gene expression, supporting the model that Ssn3 is a negative regulator of Flo8. Interestingly, deletion of the *S. cerevisiae* histone methyltransferase *JHD2* and *SSN8* results in constitutive filamentous growth that requires the transcriptional positive regulator of invasive growth, *FLO8* (10). Our finding of 288 transcripts meeting our criteria for a statistically significant change in abundance upon the inhibition of Ssn3 is similar to the finding of Holstege and colleagues (7, 31) in which microarray analyses in *S. cerevisiae* found ~3% of genes changed by their criteria. The effects of the $Ssn3^{AS}$ variant were modest compared to the effects of Ssn3 inhibition indicating the utility of this variant for the study of short term effects of Ssn3 inhibition.

In addition to Flo8, numerous of other transcriptional regulators of morphology have been described including Efg1, Cph1 (a homolog of *S. cerevisiae* Ste12, a known Ssn3 target), Tec1, Ndt80, and Ume6, and repressors like Tup1 and Nrg1 (32-39). Of these, Efg1 and Ndt80 were found to have significantly depleted phosphopeptides upon Ssn3 inhibition. We prioritized Flo8 because Wartenberg, *et al.* (14) recovered filamentation in a macrophage-evolved strain with $ssn3^{R352N}$ in an *efg1/cph1* null strain

321 background, suggesting that regulators other than these were active upon changes in
322 Cdk8 activity. Further, we showed that in embedded growth assays, the
323 hyperfilamenation phenotype in both the *ssn3* and *efg1* null backgrounds required Flo8,
324 underscoring the importance of Flo8 in Efg1-independent filamentation. Identification and
325 functional characterization of phosphorylation sites and the understanding of their roles
326 in Ssn3 regulation of activity merits further investigation. Flo8 has been implicated in the
327 transcriptional regulation of true hyphal growth in *C. albicans*, with Flo8, and its binding
328 partner Mss11, both having been described to directly bind the Hyphal Control Region in
329 the promoter of *HWP1*, one of the most strongly differentially abundant transcripts in our
330 transcriptomic data, and Flo8 is thought to be downstream of PKA (27, 40, 41). Ssn3 may
331 play an important role in coordinating the response of multiple regulators during the
332 induction and repression of filamentation. A recent study identified Ssn3 dependent
333 phosphorylation of the transcription factor Ume6 and its degradation, under conditions of
334 hypoxia and atmospheric CO_2, as one way in which the kinase can impact filamentation
335 (15). The absence of Ume6 phosphopeptides in our could be due to differences in kinetics
336 of Flo8 and Ume6 or differences in the technologies used.
337 In addition to hyperfilamentation, wrinkled colony formation and medium
338 alkalinization are phenotypes associated with *ssn3* deletion. As for hyperfilamentous
339 growth, deletion of *FLO8* suppressed the hyperalkalinization phenotype of the *ssn3*Δ/Δ
340 strain. Additionally, we were able to establish a role for Ssn3 upstream of the metabolic
341 regulator Stp2 as deletion of *STP2* in the *ssn3* background was able to almost completely
342 ablate the hyperalkalinization phenotype of the *ssn3*Δ/Δ. Stp2-mediated medium
343 alkalinization is a mechanism by which *C. albicans* can regulate its morphology thus our

findings are consistent with a model in which Ssn3 has both direct (Flo8-mediated) and indirect (Stp2-mediated) roles in determining morphology (42).

Several other pathways were identified as being influenced by Ssn3 in the proteomics studies including MAP kinase pathways, protein synthesis and chromatin regulation. It is interesting to note that studies of the human Cdk8 have also implicated it in regulating MAPK pathways (43). Notably, many of the phosphoproteins impacted by our inhibition of Ssn3 are not canonically nuclear, suggesting that Cdk8 may have a cytosolic role. This is in agreement with the work of Chen and Noble who identified a role of Cdk8 in the cytosolic phosphorylation of Sef1 (21). As an aside, we did not observe Sef1 phosphopeptides, a documented Ssn3 phosphotarget, and we speculate that this is due to the fact that our experiments were performed in an iron-replete medium which suppresses this phosphorylation event (21). We observed changes in proteins within MAP kinase cascades, their regulators, and effectors, and notable within that classification was the Hog1 MAP kinase pathway (**Table S3**). Among the depleted phosphopeptides in the *ssn3*^{AS} strain were Ssk2 and Pbs2, the MAPKKK and MAPKK, respectively, of the Hog1 pathway, but Hog1 itself was not identified as being changed upon inhibition of Ssn3 activity. We also found differences in ribosomal biogenesis and protein synthesis. Lastly, we found that phosphopeptides involved in the remodeling of chromatin, such as the Set3 histone deacetylase, were depleted upon inhibition of Cdk8 kinase activity. This is similar to a phosphoproteomic study in human cells that identified elements of the NuA3 and NuA4 histone acetyltransferase complex amongst the depleted phosphopeptides upon inhibition of Cdk8 and the related kinase Cdk19 by cortistatin A (44). Set3 is also involved in morphological determination, with a *set3* null mutant displaying a hyperfilamentous

phenotype (45). Additionally, it has been found that alterations in chromatin architecture participate in the interplay between Nrg1 and hypha-specific gene expression (39). The existence of a substantial suite of proteins involved in chromatin remodeling that show decreased phosphorylation with Ssn3 inhibition in the phosphoproteomic results is also a possible mechanism to account for the hyphal morphology phenotype of Ssn3 inhibition. A potential hypothesis is that Cdk8 phosphorylates hyphal transcriptional regulators like Flo8 acting in concert with phosphorylation of elements of the chromatin remodeling machinery, which promotes the formation of repressive chromatin structures at hypha-associated genes.

Unlike some other components of Mediator, which have pleiotropic effects on transcription, the role of the Cdk8 sub-module seems to be specific to certain developmental and nutrient regulated pathways across eukarya (22). This more specialized role has made Cdk8 a potential drug target for several diseases. For example, inhibitors of mammalian Cdk8 have been extensively explored as potential cancer therapies (46). As cancer therapeutics are often administered in the context of immunosuppression, it is important to understand the impact of these compounds on *C. albicans*, since inhibition of Ssn3 could potentiate or attenuate the virulence of this opportunistic pathogen.

Materials and Methods

Media and growth conditions: Strains were maintained on YPD plates, and overnight cultures for morphology and RNA seq were grown in YNB/1% glucose at 30°C in culture tubes on a roller drum. YPD plates were routinely streaked from glycerol stocks, and

experiments were only conducted with overnight cultures from plates not more than 5 days old. YNB medium with 2% (w/v) casamino acids and 11 mM glucose (YNBAG) with or without 5 mM N-acetyl glucosamine (GlcNAc) was adjusted to pH 5.1 (morphology and RNA seq experiments) or pH 6.0 (phosphoproteomics) with concentrated hydrochloric acid, and filter sterilized. When indicated, the pH indicator bromocresol purple was included in the medium as described in (12). Additional medium, temperature, and incubation time details pertaining to morphology assessments can be found in the corresponding figure legends.

Wrinkled colony and alkalinization assays: Overnight cultures (YPD) of each strain were washed once with water and diluted to OD_{600} 4. 8 µL of cell suspension was spotted onto the indicated medium. Images were typically taken after 2 days growth at 37°C or 3 days growth at 30°C. For alkalinization assays, 2X YNB based media was adjusted to pH 5.0 by HCl, filter sterilized and mixed with autoclaved 4% agar solution. Bromocresol purple (BCP) was added to 0.01% from a 0.1% aqueous stock into the media before 2 mL was aliquoted into each well of a 24-well plate. pH references were generated using YNB media buffered by phosphate buffer (20 mM) with known pH.

Strain construction: All strains used in this study are listed in Table S1. Primers and plasmid sequences are available upon request. Strains expressing analog-sensitive and kinase-dead Ssn3 variants, referred to as *ssn3*^{AS} and *ssn3*^{KD}, respectively, were generated by transformation of SC5314 with a DNA fragment containing *ssn3*-F257G (*ssn3*^{AS}) or *ssn3*^{D325A} (*ssn3*^{KD}) adjacent to the SAT-FLP cassette directed to the *SSN3*

413 locus. These constructs were transformed alongside the *Candida*-optimized
414 CRISPR/Cas9 machinery and a guide sequence targeting the nuclease to the *SSN3* open
415 reading frame (47). Transformants were selected on YPD with 200 µg neourseothricin
416 (GoldBio). Resistant colonies were patched onto YPD with 200 µg neourseothricin. No
417 homozygous mutant transformants were identified, likely due to the guide sequence
418 targeting the CRISPR/Cas9 nuclease to the mutant repair template. However, there were
419 transformants likely for the intended point mutation (assayed with Sanger sequencing)
420 which probably came about due to CRISPR-independent allelic replacement by
421 homologous recombination in cells that did not also take up the Cas9 machinery.
422 Amplification using primers that spanned the *SSN3* locus from DNA isolated from these
423 heterozygotes revealed the *SAT1* marker was excised during outgrowth on YPD.
424 Transformants were purified to single colonies, and neourseothricin sensitivity was
425 confirmed by patching on YPD plates containing 200 µg per mL neourseothricin.
426 Heterozygous point mutants underwent a second transformation with the same construct
427 using the methods described above to generate homozygotes. Transformants in both
428 rounds of transformation were confirmed by PCR amplifying a ≈970 base pair internal
429 region of *SSN3* covering the region encoding residues 257 and 325 using primers Ssn3
430 Internal FWD and Ssn3 Internal Rev, and Sanger sequencing with the reverse primer. As
431 in the first round, a number of these transformants had excised the resistance marker as
432 observed by PCR during outgrowth on nourseothricin plates, and these sensitive
433 homozygotes were purified to single colonies. Generation of subsequent knockout
434 mutants was carried out using a previously described transient CRISPR-Cas9 system
435 using a SAT-flipper selection marker (48). To generate double mutants, the *SAT1*

436 cassette was recycled by inducing flippase expression in YP maltose (1% yeast extract,
437 2% peptone, 2% maltose) for 24 hours. Generation of HA-tagged flo8-bearing strains
438 was similarly accomplished through a repair construct in which the desired allele was
439 fused to the SAT-FLP marker.
440
441 *Mediator purification and in vitro kinase assays:* Ssn8-tagged Mediator containing various
442 Cdk8 alleles was purified and used for *in vitro* kinase assays with a GST-CTD substrate
443 as previously described (20, 49). Amounts of the kinase were normalized by the signal
444 on the FLAG tag.
445
446 *Analysis of C. albicans morphology*: Morphological assessment was conducted in
447 $YNBNAG_{11}$ at 30°C. For the analysis of the effects of 3-MB-PP1 (the ATP analog used
448 to inhibit analog-sensitive kinases), cells grown overnight at 30°C in YNB with 1% (w/v)
449 glucose were pelleted by centrifugation and resuspended in 5 mL $YNBNAG_{11}$ pH 5.1
450 containing 5 μM 3-MB-PP1 (EMD MILLIPORE) or DMSO as a vehicle control. The cells
451 were then incubated at 30°C for 3h in culture tubes on a roller drum, fixed in
452 formaldehyde, and morphology quantified from image captured using differential
453 interference contrast microscopy. Cells were considered to be true hyphae if germ tubes
454 had parallel sides and no invagination at the junction of the filament and the mother
455 blastospore. A minimum of 175 cells per replicate were counted, and data presented
456 represent three independent biological replicates conducted on three different days.
457 Cultures were inoculated to an initial density of $1x10^7$ cells per mL.
458

459 *Analysis of the C. albicans transcriptome upon Ssn3 inhibition using RNA seq*: Cells were
460 grown as described above for morphological assessment, but the incubation time was
461 reduced to decrease indirect effects of Ssn3 inhibition. Specifically, the time following
462 drug exposure was reduced from three hours to one hour. The 5 mL cultures were
463 collected one hour after 3-MB-PP1 addition, pelleted by centrifugation, snap frozen in
464 liquid nitrogen, and RNA was isolated with the MasterPure™ Yeast RNA Purication Kit
465 (Epicentre MPY03100). For RNA sequencing, 500 ng of total RNA was input into the Kapa
466 mRNA HyperPrep kit (Kapa Biosystems, Wilmington, MA) and processed according to
467 the manufacturer's instructions. All 24 samples were multiplexed together into a single
468 High Output 2x75bp run on a NextSeq 500 instrument (Illumina, San Diego, CA). Raw
469 reads were mapped to the *C. albicans* genome SC5314 (version A21-s02-m09-r04,
470 candidagenome.org), and normalized using EdgeR. KEGG enrichment analysis was
471 carried out using KOBAS 2.0 (50).
472
473 RNA was extracted from frozen cell pellets as described (51). Data were presented after
474 normalization by geometric mean of positive controls and geometric mean of *TEF1* and
475 *ACT1* reads. Gene expression in a wild-type strain or a *flo8* mutant was set to '1' as
476 mentioned in the figure legends. The accession number for the data is GSE171859.
477 During the review phase, RNA Seq data can be accessed at
478 https://www.ncbi.nlm.nih.gov/geo/query/acc.cgi?acc=GSE171859 and the access token
479 is mpsfuucitvktreh. The data will be publicly available upon acceptance for publication.
480

Ssn3 phosphoproteomic experimental design: 300 mL $YNBNAG_{11}$ (pH 6.0) cultures of SC5314 and *ssn3*^{AS} were inoculated at a density of OD_{600} of 0.01 and grown to OD_{600} of 4.5 in flasks with shaking at 30°C, then incubated for a subsequent 4.5 hours to ensure cells had entered stationary phase. Stationary phase cells were incubated in the presence of 5 μM 3-MB-PP1 for five minutes to enable drug entry into the cell. The cells were then concentrated and added to fresh, pre-warmed medium containing either drug or vehicle and incubated for 15 minutes at 30°C with shaking. Either DMSO vehicle or 5 μM 3-MB-PP1 was then added, after which cultures were incubated with shaking for five minutes at 30°C. Then, 1.2 L of prewarmed fresh $YNBNAG_{11}$ (pH 6.0) medium was added as a 1.25X concentrate, and cells were incubated for an additional 15 minutes. The cells were then harvested by centrifugation and cell lysis by grinding under liquid nitrogen. All growth and incubation steps were conducted at 30°C, and the data represent the average of three independent replicates conducted on three separate days.

*Phosphoproteomic analysis***.** Yeast powder was lysed in ice-cold lysis buffer ((8 M urea, 25 mM Tris-HCl pH 8.6, 150 mM NaCl, phosphatase inhibitors (2.5 mM beta-glycerophosphate, 1 mM sodium fluoride, 1 mM sodium orthovanadate, 1 mM sodium molybdate) and protease inhibitors (1 mini-Complete EDTA-free tablet per 10 ml lysis buffer; Roche Life Sciences)) and sonicated three times for 15 sec each with intermittent cooling on ice. Lysates were centrifuged at 15,000 x *g* for 30 minutes at 4˚C. Supernatants were transferred to a new tube and the protein concentration was determined using a BCA assay (Pierce-ThermoFisher Scientific). For reduction, DTT was added to the lysates to a final concentration of 5 mM and incubated for 30 min at 55˚C. Afterwards,

lysates were cooled to room temperate and alkylated with 15 mM iodoacetamide at room temperature for 45 min. The alkylation was then quenched by the addition of an additional 5 mM DTT. After 6-fold dilution with 25 mM Tris-HCl pH 8, the samples were digested overnight at 37˚C with 1:100 (w/w) trypsin. The next day, the digest was stopped by the addition of 0.25% TFA (final v/v), centrifuged at 3500 x *g* for 30 minutes at room temperature to pellet precipitated lipids, and peptides were desalted on a 500 mg (sorbent weight) SPE C_{18} cartridge (Grace-Davidson). Peptides were lyophilized and stored at -80˚C until needed for future use.

*Phosphopeptide enrichment***.** Phosphopeptide purification was performed as previously described (52). Briefly, peptides were resuspended in 1.5 M lactic acid in 50% ACN ("binding solution"). Titanium dioxide microspheres were added and vortexed by affixing to the top of a vortex mixer on the highest speed setting at room temperature for 1 hour. Afterwards, microspheres were washed twice with binding solution and three times with 50% ACN / 0.1% TFA. Peptides were eluted twice with 50 mM KH_2PO_4 (adjusted to pH 10 with ammonium hydroxide). Peptide eluates were combined, quenched with 50% ACN / 5% formic acid, dried and desalted on a µHLB OASIS C_{18} desalting plate (Waters). Phosphopeptide enrichment was repeated once.

TMT-labeling. Phosphopeptides were resuspended in 133 mM HEPES (Sigma) pH 8.5 and 20% acetonitrile (ACN) (Burdick & Jackson). Peptides were transferred to dried, individual TMT reagent (ThermoFisher Scientific), and vortexed to mix reagent and peptides. After 1 hr at room temperature, each reaction was quenched with 3 µl of 500

527 mM ammonium bicarbonate solution for 10 minutes, mixed, diluted 3-fold with 0.1% TFA
528 in water, and desalted using C_{18} solid phase extraction cartridges (ThermoFisher
529 Scientific). The desalted multiplexes were dried by vacuum centrifugation.
530
531 *Pentafluorophenyl-based Reversed Phase HPLC.* Offline PFP-based reversed phase
532 HPLC fractionation was performed as previously described (53). Briefly, phosphopeptides
533 were fractionated using a Waters XSelect HSS PFP 2.5 µm 2.1 × 150 mm column on an
534 Agilent 1100 liquid chromatography system, buffer A was 3% acetonitrile / 0.1% TFA, and
535 buffer B was 95% acetonitrile / 0.1% TFA. Flow rate was 150 µl/min with a constant
536 column temperature of 20˚C. Phosphopeptides were fractioned using a 60-minute linear
537 gradient from 8-45% acetonitrile and collected as 48 fractions between minutes 2 and 65.
538 The 48 fractions were then combined into 24 total samples.
539
540 *TMT-based quantitative data analysis* TMT-labeled samples were analyzed on a Orbitrap
541 Fusion (Senko, Remes et al. 2013) mass spectrometer (ThermoScientific) equipped with
542 an Easy-nLC 1000 (ThermoScientific). Peptides were resuspended in 8% methanol / 1%
543 formic acid across a column (45 cm length, 100 µm inner diameter, ReproSil, C_{18} AQ 1.8
544 µm 120 Å pore) pulled in-house across a 2 h gradient from 8% acetonitrile/0.0625% formic
545 acid to 37% acetonitrile/0.0625% formic acid. The Orbitrap Fusion was operated in data-
546 dependent, SPS-MS3 quantification mode (54, 55) wherein an Orbitrap MS1 scan was
547 taken (scan range = 350 – 1500 m/z, R = 120K, AGC target = 2.5e5, max ion injection
548 time = 100 ms), followed by ion trap MS2 scans on the most abundant precursors for 4

549 seconds (max speed mode, quadrupole isolation = 0.6 m/z, AGC target = 4e3, scan rate
550 = rapid, max ion injection time = 60 ms, minimum MS1 scan signal = 5e5 normalized
551 units, charge states = 2, 3 and 4 included, CID collision energy = 33%) and Orbitrap MS3
552 scans for quantification (R = 15K, AGC target = 2e4, max ion injection time = 125 ms,
553 HCD collision energy = 48%, scan range = 120 – 140 m/z, synchronous precursors
554 selected = 10). The raw data files were searched using COMET with a static mass of
555 229.162932 on peptide N-termini and lysines and 57.02146 Da on cysteines, and a
556 variable mass of 15.99491 Da on methionines and 79.96633 Da on serines, threonines
557 and tyrosine against the target-decoy version of the respective FASTA database (UniProt;
558 www.uniprot.org) and filtered to a <1% FDR at the peptide level. Quantification of LC-
559 MS/MS spectra was performed using software developed in house. Phosphopeptide
560 intensities were adjusted based on total TMT reporter ion intensity in each channel and
561 $\log_2$ transformed. P-values were calculated using a two tailed Student's t-test assuming
562 unequal variance.
563

References:

1. Dannappel MV, Sooraj D, Loh JJ, Firestein R. 2018. Molecular and in vivo functions of the CDK8 and CDK19 kinase modules. Front Cell Dev Biol 6:171.

2. Youn DY, Xiaoli AM, Pessin JE, Yang F. 2016. Regulation of metabolism by the Mediator complex. Biophys Rep 2:69-77.

3. Galbraith MD, Andrysik Z, Pandey A, Hoh M, Bonner EA, Hill AA, Sullivan KD, Espinosa JM. 2017. CDK8 kinase activity promotes glycolysis. Cell Rep 21:1495-1506.

4. Bancerek J, Poss ZC, Steinparzer I, Sedlyarov V, Pfaffenwimmer T, Mikulic I, Dolken L, Strobl B, Muller M, Taatjes DJ, Kovarik P. 2013. CDK8 kinase phosphorylates transcription factor STAT1 to selectively regulate the interferon response. Immunity 38:250-62.

5. Zhao X, Feng D, Wang Q, Abdulla A, Xie XJ, Zhou J, Sun Y, Yang ES, Liu LP, Vaitheesvaran B, Bridges L, Kurland IJ, Strich R, Ni JQ, Wang C, Ericsson J, Pessin JE, Ji JY, Yang F. 2012. Regulation of lipogenesis by cyclin-dependent kinase 8-mediated control of SREBP-1. J Clin Invest 122:2417-27.

6. Rohde JR, Trinh J, Sadowski I. 2000. Multiple signals regulate GAL transcription in yeast. Mol Cell Biol 20:3880-6.

583 7. Holstege FC, Jennings EG, Wyrick JJ, Lee TI, Hengartner CJ, Green MR, Golub
584 TR, Lander ES, Young RA. 1998. Dissecting the regulatory circuitry of a eukaryotic
585 genome. Cell 95:717-28.

586 8. Nelson C, Goto S, Lund K, Hung W, Sadowski I. 2003. Srb10/Cdk8 regulates yeast
587 filamentous growth by phosphorylating the transcription factor Ste12. Nature
588 421:187-90.

589 9. Raithatha S, Su TC, Lourenco P, Goto S, Sadowski I. 2012. Cdk8 regulates
590 stability of the transcription factor Phd1 to control pseudohyphal differentiation of
591 Saccharomyces cerevisiae. Mol Cell Biol 32:664-74.

592 10. Law MJ, Ciccaglione K. 2015. Fine-tuning of histone H3 Lys4 methylation during
593 pseudohyphal differentiation by the CDK submodule of RNA polymerase II.
594 Genetics 199:435-53.

595 11. Liu Z, Myers LC. 2017. *Candida albicans* Swi/Snf and Mediator complexes
596 differentially regulate Mrr1-induced *MDR1* expression and fluconazole resistance.
597 Antimicrob Agents Chemother 61.

598 12. Lindsay AK, Morales DK, Liu Z, Grahl N, Zhang A, Willger SD, Myers LC, Hogan
599 DA. 2014. Analysis of *Candida albicans* mutants defective in the Cdk8 module of
600 mediator reveal links between metabolism and biofilm formation. PLoS Genet
601 10:e1004567.

602 13. Grahl N, Demers EG, Lindsay AK, Harty CE, Willger SD, Piispanen AE, Hogan
603 DA. 2015. Mitochondrial activity and Cyr1 are key regulators of Ras1 activation of
604 *C. albicans* virulence pathways. PLoS Pathog 11:e1005133.

605 14. Wartenberg A, Linde J, Martin R, Schreiner M, Horn F, Jacobsen ID, Jenull S, Wolf
606 T, Kuchler K, Guthke R, Kurzai O, Forche A, d'Enfert C, Brunke S, Hube B. 2014.
607 Microevolution of *Candida albicans* in macrophages restores filamentation in a
608 nonfilamentous mutant. PLoS Genet 10:e1004824.

609 15. Lu Y, Su C, Ray S, Yuan Y, Liu H. 2019. CO2 signaling through the Ptc2-Ssn3
610 axis governs sustained hyphal development of *Candida albicans* by reducing
611 Ume6 phosphorylation and degradation. mBio 10.

612 16. Liu Y, Kung C, Fishburn J, Ansari AZ, Shokat KM, Hahn S. 2004. Two cyclin-
613 dependent kinases promote RNA polymerase II transcription and formation of the
614 scaffold complex. Mol Cell Biol 24:1721-35.

615 17. Cao F, Lane S, Raniga PP, Lu Y, Zhou Z, Ramon K, Chen J, Liu H. 2006. The Flo8
616 transcription factor is essential for hyphal development and virulence in *Candida*
617 *albicans*. Mol Biol Cell 17:295-307.

618 18. Polvi EJ, Veri AO, Liu Z, Hossain S, Hyde S, Kim SH, Tebbji F, Sellam A, Todd
619 RT, Xie JL, Lin ZY, Wong CJ, Shapiro RS, Whiteway M, Robbins N, Gingras AC,
620 Selmecki A, Cowen LE. 2019. Functional divergence of a global regulatory
621 complex governing fungal filamentation. PLoS Genet 15:e1007901.

622 19. Bishop AC, Ubersax JA, Petsch DT, Matheos DP, Gray NS, Blethrow J, Shimizu
623 E, Tsien JZ, Schultz PG, Rose MD, Wood JL, Morgan DO, Shokat KM. 2000. A
624 chemical switch for inhibitor-sensitive alleles of any protein kinase. Nature
625 407:395-401.

626 20. Willger SD, Liu Z, Olarte RA, Adamo ME, Stajich JE, Myers LC, Kettenbach AN,
627 Hogan DA. 2015. Analysis of the *Candida albicans* phosphoproteome. Eukaryot
628 Cell 14:474-85.

629 21. Chen C, Noble SM. 2012. Post-transcriptional regulation of the Sef1 transcription
630 factor controls the virulence of *Candida albicans* in its mammalian host. PLoS
631 Pathog 8:e1002956.

632 22. Allen BL, Taatjes DJ. 2015. The Mediator complex: a central integrator of
633 transcription. Nat Rev Mol Cell Biol 16:155-66.

634 23. Martin R, Albrecht-Eckardt D, Brunke S, Hube B, Hunniger K, Kurzai O. 2013. A
635 core filamentation response network in Candida albicans is restricted to eight
636 genes. PLoS One 8:e58613.

637 24. Malumbres M. 2014. Cyclin-dependent kinases. Genome Biol 15:122.

638 25. Kemp BE, Graves DJ, Benjamini E, Krebs EG. 1977. Role of multiple basic
639 residues in determining the substrate specificity of cyclic AMP-dependent protein
640 kinase. J Biol Chem 252:4888-94.

641 26. UniProt C. 2019. UniProt: a worldwide hub of protein knowledge. Nucleic Acids
642 Res 47:D506-D515.

643 27. Liu H, Styles CA, Fink GR. 1996. *Saccharomyces cerevisiae* S288C has a
644 mutation in FLO8, a gene required for filamentous growth. Genetics 144:967-78.

645 28. Doedt T, Krishnamurthy S, Bockmuhl DP, Tebarth B, Stempel C, Russell CL,
646 Brown AJ, Ernst JF. 2004. APSES proteins regulate morphogenesis and
647 metabolism in *Candida albicans*. Mol Biol Cell 15:3167-80.

648 29. Saputo S, Kumar A, Krysan DJ. 2014. Efg1 directly regulates *ACE2* expression to
649 mediate cross talk between the cAMP/PKA and RAM pathways during *Candida*
650 *albicans* morphogenesis. Eukaryot Cell 13:1169-80.

651 30. Miramon P, Pountain AW, van Hoof A, Lorenz MC. 2020. The Paralogous
652 Transcription Factors Stp1 and Stp2 of *Candida albicans* Have Distinct Functions
653 in Nutrient Acquisition and Host Interaction. Infect Immun 88.

654 31. van de Peppel J, Kettelarij N, van Bakel H, Kockelkorn TT, van Leenen D, Holstege
655 FC. 2005. Mediator expression profiling epistasis reveals a signal transduction
656 pathway with antagonistic submodules and highly specific downstream targets.
657 Mol Cell 19:511-22.

658 32. Schweizer A, Rupp S, Taylor BN, Rollinghoff M, Schroppel K. 2000. The
659 TEA/ATTS transcription factor CaTec1p regulates hyphal development and
660 virulence in Candida albicans. Mol Microbiol 38:435-45.

661 33. Stoldt VR, Sonneborn A, Leuker CE, Ernst JF. 1997. Efg1p, an essential regulator
662 of morphogenesis of the human pathogen *Candida albicans*, is a member of a
663 conserved class of bHLH proteins regulating morphogenetic processes in fungi.
664 Embo J 16:1982-91.

665 34. Liu H, Kohler J, Fink GR. 1994. Suppression of hyphal formation in *Candida*
666 *albicans* by mutation of a *STE12* homolog. Science 266:1723-6.

667 35. Braun BR, Johnson AD. 1997. Control of filament formation in *Candida albicans*
668 by the transcriptional repressor TUP1. Science 277:105-9.

669 36. Min K, Biermann A, Hogan DA, Konopka JB. 2018. Genetic analysis of NDT80
670 family transcription factors in *Candida albicans* using new CRISPR-Cas9
671 approaches. mSphere 3: 00545-18.

672 37. Murad AM, Leng P, Straffon M, Wishart J, Macaskill S, MacCallum D, Schnell N,
673 Talibi D, Marechal D, Tekaia F, d'Enfert C, Gaillardin C, Odds FC, Brown AJ. 2001.
674 *NRG1* represses yeast-hypha morphogenesis and hypha-specific gene
675 expression in *Candida albicans*. EMBO J 20:4742-52.

676 38. Banerjee M, Thompson DS, Lazzell A, Carlisle PL, Pierce C, Monteagudo C,
677 Lopez-Ribot JL, Kadosh D. 2008. UME6, a novel filament-specific regulator of
678 *Candida albicans* hyphal extension and virulence. Mol Biol Cell 19:1354-65.

679 39. Lu Y, Su C, Wang A, Liu H. 2011. Hyphal development in *Candida albicans*
680 requires two temporally linked changes in promoter chromatin for initiation and
681 maintenance. PLoS Biol 9:e1001105.

682 40. Su C, Li Y, Lu Y, Chen J. 2009. Mss11, a transcriptional activator, is required for
683 hyphal development in Candida albicans. Eukaryot Cell 8:1780-91.

684 41. Pan X, Heitman J. 2002. Protein kinase A operates a molecular switch that governs
685 yeast pseudohyphal differentiation. Mol Cell Biol 22:3981-93.

686 42. Vylkova S, Carman AJ, Danhof HA, Collette JR, Zhou H, Lorenz MC. 2011. The
687 fungal pathogen *Candida albicans* autoinduces hyphal morphogenesis by raising
688 extracellular pH. mBio 2:e00055-11.

689 43. Donner AJ, Ebmeier CC, Taatjes DJ, Espinosa JM. 2010. CDK8 is a positive
690 regulator of transcriptional elongation within the serum response network. Nat
691 Struct Mol Biol 17:194-201.

692 44. Poss ZC, Ebmeier CC, Odell AT, Tangpeerachaikul A, Lee T, Pelish HE, Shair
693 MD, Dowell RD, Old WM, Taatjes DJ. 2016. Identification of Mediator Kinase
694 Substrates in Human Cells using Cortistatin A and Quantitative
695 Phosphoproteomics. Cell Rep 15:436-50.

696 45. Hnisz D, Majer O, Frohner IE, Komnenovic V, Kuchler K. 2010. The Set3/Hos2
697 histone deacetylase complex attenuates cAMP/PKA signaling to regulate
698 morphogenesis and virulence of *Candida albicans*. PLoS Pathog 6:e1000889.

699 46. Philip S, Kumarasiri M, Teo T, Yu M, Wang S. 2018. Cyclin-Dependent Kinase 8:
700 A New Hope in Targeted Cancer Therapy? J Med Chem 61:5073-5092.

47. Min K, Ichikawa Y, Woolford CA, Mitchell AP. 2016. *Candida albicans* gene deletion with a transient CRISPR-Cas9 system. mSphere 1.

48. Grahl N, Demers EG, Crocker AW, Hogan DA. 2017. Use of RNA-Protein complexes for genome editing in non-albicans *Candida* species. mSphere 2.

49. Guidi BW, Bjornsdottir G, Hopkins DC, Lacomis L, Erdjument-Bromage H, Tempst P, Myers LC. 2004. Mutual targeting of mediator and the TFIIH kinase Kin28. J Biol Chem 279:29114-20.

50. Xie C, Mao X, Huang J, Ding Y, Wu J, Dong S, Kong L, Gao G, Li CY, Wei L. 2011. KOBAS 2.0: a web server for annotation and identification of enriched pathways and diseases. Nucleic Acids Res 39:W316-22.

51. Zhang A, Liu Z, Myers LC. 2013. Differential regulation of white-opaque switching by individual subunits of *Candida albicans* mediator. Eukaryot Cell 12:1293-304.

52. Kettenbach AN, Gerber SA. 2011. Rapid and reproducible single-stage phosphopeptide enrichment of complex peptide mixtures: application to general and phosphotyrosine-specific phosphoproteomics experiments. Anal Chem 83:7635-44.

53. Grassetti AV, Hards R, Gerber SA. 2017. Offline pentafluorophenyl (PFP)-RP prefractionation as an alternative to high-pH RP for comprehensive LC-MS/MS proteomics and phosphoproteomics. Anal Bioanal Chem 409:4615-4625.

720 54. Ting L, Rad R, Gygi SP, Haas W. 2011. MS3 eliminates ratio distortion in isobaric
721 multiplexed quantitative proteomics. Nat Methods 8:937-40.

722 55. McAlister GC, Nusinow DP, Jedrychowski MP, Wuhr M, Huttlin EL, Erickson BK,
723 Rad R, Haas W, Gygi SP. 2014. MultiNotch MS3 enables accurate, sensitive, and
724 multiplexed detection of differential expression across cancer cell line proteomes.
725 Anal Chem 86:7150-8.

726

Acknowledgments

Research reported in this publication was supported by National Institute of Health (NIH) through the National Institute of Allergy and Infectious Disease grants AI127548 to D.A.H., AI115253 to L.C. M., and T32 AI007519 to J.M.H. and National Institute for General Medical Science grant R35 GM119455 for A.N.K.. This work was also supported by P30-DK117469 for the Applied Bioinformatics and Biostatistics Core. Sequencing services and specialized equipment was provided by the Genomics and Molecular Biology Shared Resource Core at Dartmouth supported by NCI Cancer Center Support Grant 5P30CA023108-37. Equipment used was supported by the NIH IDeA award to Dartmouth BioMT P20-GM113132. The content is solely the responsibility of the authors and does not necessarily represent the official views of the NIH.

740 **Tables:**

741

742

	Down > 2-fold	Up > 2-fold	Total Down	Total Up
743 Total phosphopeptides	977	264	2967	2522
Total phosphoproteins	552	202	1165	1057
744 S/T#P motif phosphopeptides	293	94	943	867
S/T#P motif phosphoproteins	218	77	505	493

745

746 **Table 1**. Summary of phosphopeptides and phosphoproteins detected by motif.
747 Analysis limited to those peptides to which P-values of <0.05 were assigned in the
748 comparison of *ssn3*^{AS} to SC5134 wild type (WT). Down indicates phosphopeptides
749 lower in *ssn3*^{AS} treated with 3-MB-PP1 compared to WT treated with 3-MB-PP1; up
750 indicates phosphopeptides that were more abundant in the *ssn3*^{AS} strain treated with 3-
751 MB-PP1 compared to WT treated with 3-MB-PP1. The total refers to the number of
752 peptides or proteins that are significantly different regardless of fold-difference. "#"
753 indicates the detected phosphorylation on a serine or threonine, S/T, in either a -1
754 position relative to a proline, S/T#P motif.

755

Figure Legends:

Figure 1. 3-MB-PP1 inhibits the activity of analog-sensitive Ssn3^{AS}, but not Ssn3^{WT} *in vitro*. *In vitro* kinase reactions contained purified Mediator from a strain with Ssn3^{WT} or Ssn3^{AS}, ^{32}P-ATP, purified GST-tagged RNA Pol II C-terminal domain (CTD) and the indicated concentrations of 3-MB-PP1 inhibitor. Reactions were analyzed by SDS-PAGE and visualized by phosphorimaging.

Figure 2. 3-MB-PP1 stimulates hyphal growth in a strain bearing analog-sensitive alleles of *SSN3.* **A.** Morphology of wild type (WT) SC5314, *ssn3^{AS}* and *ssn3^{KD}* strains was assessed after growth in either 5 μM 3-MB-PP1 or vehicle (DMSO) for 3h at 30°C. Quantification of yeast, pseudohyphae and hyphae in cultures by microscopic analysis of blinded samples. ANOVA with multiple comparisons for the hyphal cell populations shown. ****, $p<0.001$, ns, not significant; a, $p<0.001$ for comparison to WT with 3MB-PP1; b, $p<0.001$ comparison to WT with DMSO. **B.** Representative images of cell populations from cultures analyzed in panel A.

Figure 3. Heat map for genes induced upon inhibition of Ssn3^{AS} by 3-MB-PP1. Seventy-seven genes were 2-fold higher in both the comparison of Ssn3^{AS} with 3-MB-PP1 compared to WT with 3-MB-PP1 and of Ssn3^{AS} with 3-MB-PP1 compared to with the DMSO control. The heat map shows Log2-transformed counts per million for expressed transcripts.

779 **Figure 4**. Overview of proteins for which two phosphopeptides were lower by >2 fold upon
780 inhibition of Ssn3. Focusing on peptides that were significantly lower in $Ssn3^{AS}$ treated
781 with 3-MB-PP1 relative to control cultures ($p<0.05$ FDR-corrected), we found 977
782 peptides that were 2-fold lower upon 3-MB-PP1 inhibition of *ssn3*^{AS} relative to changes in
783 SC5314 WT. Two hundred and eighteen proteins had two more peptides that met these
784 criteria, forty of which were predicted to have nuclear localization. Med4 is a validated *C.*
785 *albicans* Ssn3 target. If an alias is available for an unnamed gene, it is shown in
786 parentheses.
787
788 **Figure 5.** *SSN3* repression of filamentation is *FLO8* dependent. A. Colony morphology
789 of a wild type *C. albicans* strain (SC5314), *ssn3Δ/Δ*, *flo8Δ/Δ* and *ssn3Δ/Δ flo8Δ/Δ* strains
790 grown on YNBA agar medium alone or supplemented with 110 mM glucose at 30°C or
791 on YNBA at 37°C. B. Cell morphology of strains tested in (A) after cells were grown in
792 $YNBN_{2.5}AG_{11}$ at 30°C for 3 hours. C. NanoString analysis of indicated hypha-specific
793 genes over-expression in the SC5314 wild type, and *ssn3*Δ/Δ*, and ssn3*Δ/Δ*flo8*Δ/Δ
794 mutants. RNA was extracted from cells grown as indicated for (B) but for 75 minutes.
795 Gene expression was represented by mean and standard deviation after normalization to
796 Nanostring positive controls, and *TEF1* and *ACT1* reference transcripts; expression of
797 each gene in the wild type strain (SC5314) was set to '1'; **, $p<0.01$ and ***,$p<0.001$. D.
798 The embedded colonies of the same set of strains shown in (A) grown in YPS at 25°C.
799 **Figure 6.** Residues identified as phosphorylation sites influence Flo8 function. A.
800 SC5314 wild type, *ssn3Δ/Δ*, *flo8*Δ/Δ and *ssn3*Δ/Δ*flo8*Δ/Δ strains were imaged after growth
801 as colonies on YNBA or YNBA+110 mM glucose at 37˚C. *flo8*Δ/Δ and *ssn3*Δ/Δ*flo8*Δ/Δ

802 expressing C-terminally 3XHA tagged Flo8^{WT}, Flo8$^{T589A/S620A}$ or Flo8$^{T589E/S620E}$ were also
803 included. B. Cell morphology of SC5314, *flo8*Δ/Δ, and *flo8*Δ/Δ expressing 3XHA-tagged
804 Flo8^{WT}, Flo8^{T589A,S620A} or Flo8^{T589E,S620E} after growth in YNB$N_{2.5}$AG_{11} at 30°C for 3h. C.
805 Gene expression in *flo8*Δ/Δ expressing 3XHA-tagged Flo8^{WT} or Flo8$^{T589A/S620A}$ relative to
806 *flo8*Δ/Δ after growth in YNBNAG for ~2h. Data show the mean and standard deviation
807 from measurement on triplicate RNA samples. Gene expression in *flo8* mutant (not
808 shown) was set to '1'. P-values (t-tests) were directly denoted or indicated by '*' ($p<0.05$),
809 '**'($p<0.01$) or '***' ($p<0.001$) to show statistically significant differences. D.
810 Immunoblotting analysis with an α-HA antibody showing levels and gel mobility of native
811 Flo8 with the C-terminal 3X-HA tag or variants with T589A,S620A or T589E,S620E
812 substitutions; proteins were expressed in either *flo8*Δ/Δ or *ssn3*Δ/Δ *flo8*Δ/Δ backgrounds
813 and were grown in YNBAG at 30°C to mid-log phase. E. Flo8-HA levels in strains with full
814 Ssn3 activity, SC5314 (Ssn3^{WT}) and *ssn3^{AS}*, or without Ssn3 activity (*ssn3*Δ/Δ or *ssn3^{KD}*).
815
816 **Figure 7**. Medium alkalinization is affected by Ssn3 and Stp2. A. Comparison of medium
817 pH by growth of SC5314, *ssn3*Δ/Δ, *stp2*Δ/Δ and *ssn3*Δ/Δ *stp2*Δ/Δ strains at 37°C. B. *ssn3*
818 hyperalkalinization phenotype is dependent on *FLO8* at 37°C. SC5314, *ssn3*Δ/Δ, *flo8*Δ/Δ
819 and *ssn3*Δ/Δ*flo8*Δ/Δ alone or expressing C-terminally 3XHA tagged Flo8^{WT},
820 Flo8$^{T589A/S620A}$ or Flo8$^{T589E/S620E}$. Medium pH was assessed on YNBA with increasing
821 concentrations of glucose and bromocresol purple as a pH indicator.
822
823 **Figure S1.** *FLO8* is required for hyperfilamentation in an *efg1*Δ/Δ mutant in embedded
824 conditions and in colony biofilms. A. SC5314 wild type parental strain, *flo8*Δ/Δ, *flo8*Δ/Δ

825 complemented with *FLO8*, *efg1*Δ/Δ, *efg1*Δ/Δ*flo8*Δ/Δ, *efg1*Δ/Δ*flo8*Δ/Δ+*FLO8* as embedded
826 colonies in YPS agar 23˚C or YNBA agar with 110 mM glucose at 30˚C. The *efg1*Δ/Δ is
827 hyperfilamentous in embedded colony conditions and the filamentation is dependent on
828 *FLO8*.

Supplementary Data:

Table S1. Strains used in this work.

Table S2. RNA seq analyses to determine the effects of specific inhibition of ssn3-as by 3-MB-PP1 (drug). Sheets one and two compare the effect of drug versus vehicle in SC5314 and ssn3as, respectively.

Table S3. Phosphoproteomic analysis of the effect of 3-MB-PP1 on ssn3^{as} versus SC5314. Sheet one provides an annotated summary of phosphopeptides statistically significantly altered by drug treatment of compared to drug treatment of SC5314. Peptides highlighted in red indicate phosphorylation of a serine or threonine with a proline in the +1 or +2 position. Sheet two provides the data with each replicate of the triplicate experiment parsed individually.

Table S4. KEGG pathway enrichment analysis of transcripts altered in abundance in the *ssn3^{as}* strain by 3-MB-PP1 treatment vs vehicle.

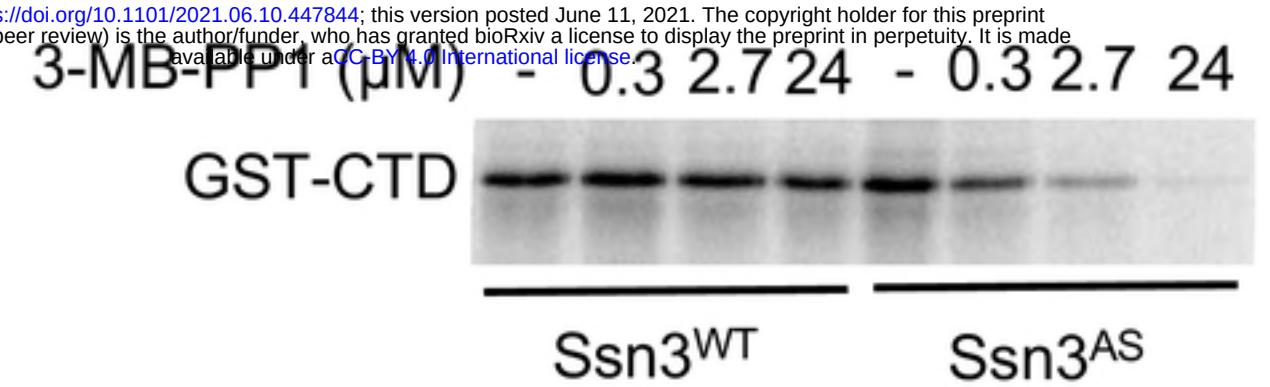

Figure 1. 3-MB-PP1 inhibits the activity of analog-sensitive Ssn3^{AS}, but not Ssn3^{WT} *in vitro*. *In vitro* kinase reactions contained purified Mediator from a strain with Ssn3^{WT} or Ssn3^{AS}, ^{32}P-ATP, purified GST-tagged RNA Pol II C-terminal domain (CTD) and the indicated concentrations of 3-MB-PP1 inhibitor. Reactions were analyzed by SDS-PAGE and visualized by phosphorimaging.

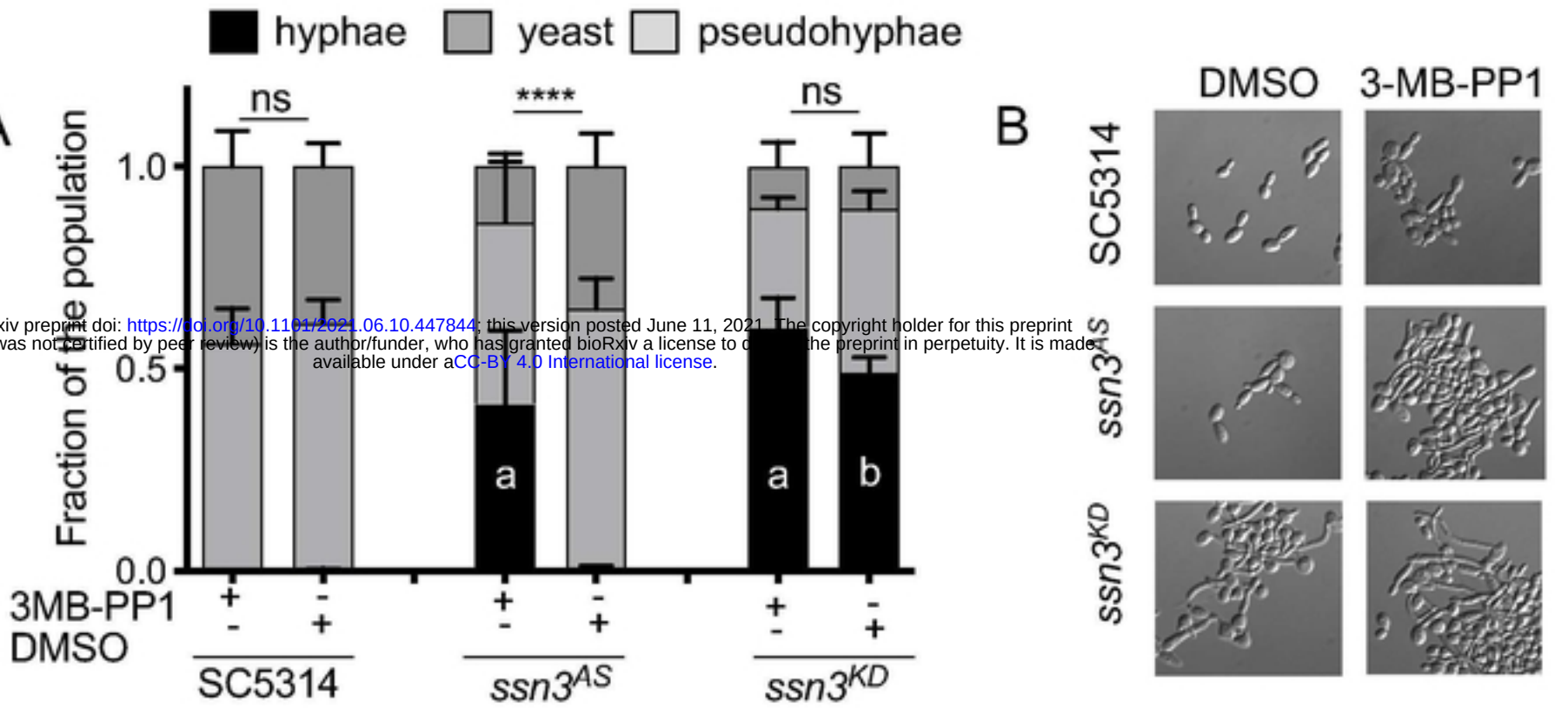

Figure 2. 3-MB-PP1 stimulates hyphal growth in a strain bearing analog-sensitive alleles of *SSN3.* **A.** Morphology of wild type (WT) SC5314, *ssn3*^{AS} and *ssn3*^{KD} strains was assessed after growth in either 5 μM 3-MB-PP1 or vehicle (DMSO) for 3h at 30°C. Quantification of yeast, pseudohyphae and hyphae in cultures by microscopic analysis of blinded samples. ANOVA with multiple comparisons for the hyphal cell populations shown. ****, p<0.001, ns, not significant; a, p<0.001 for comparison to WT with 3MB-PP1; b, p<0.001 comparison to WT with DMSO. **B.** Representative images of cell populations from cultures analyzed in panel A.

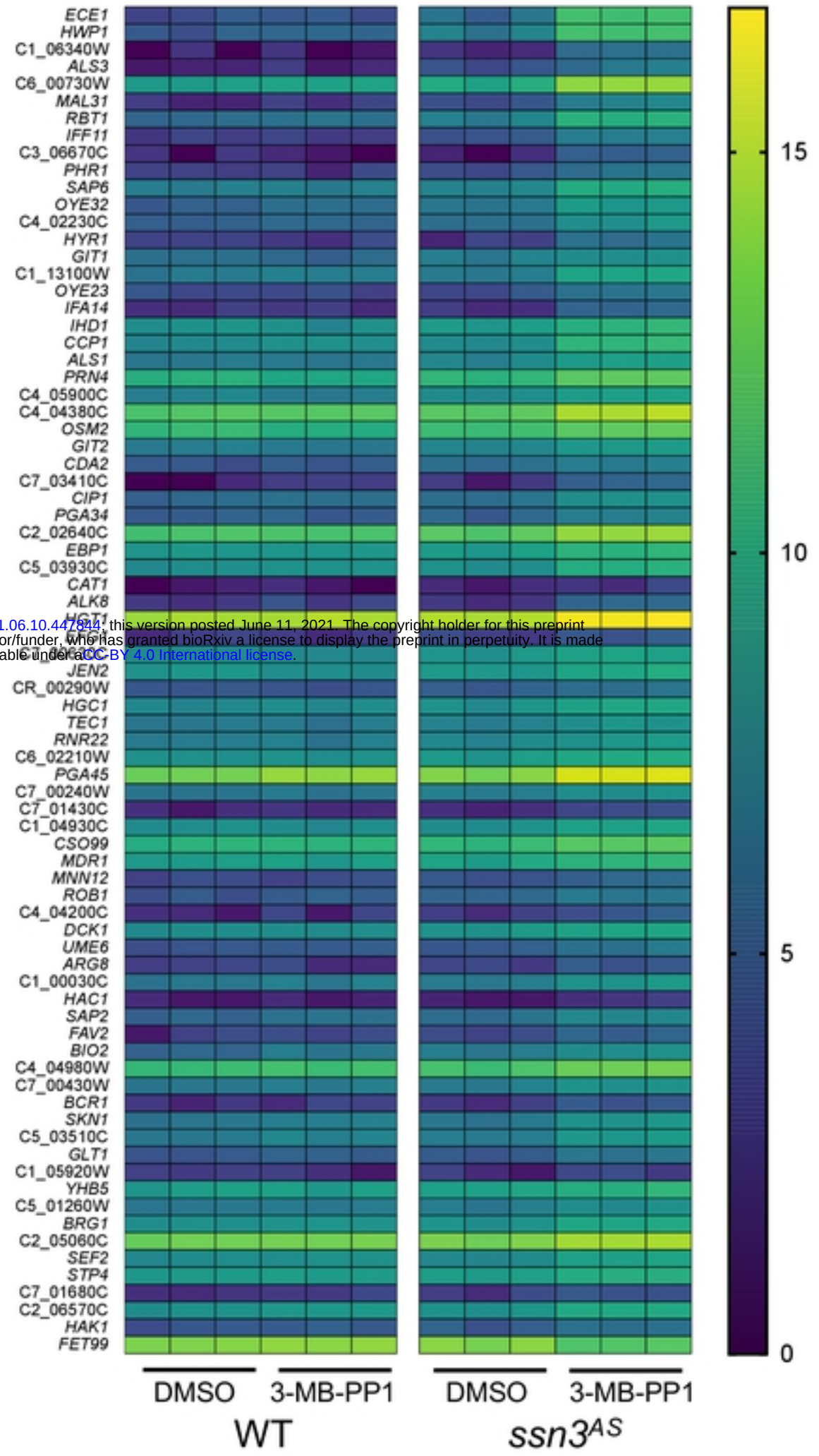

Figure 3. Heat map for genes induced upon inhibition of Ssn3^{AS} by 3-MB-PP1. Seventy-seven genes were 2-fold higher in both the comparison of Ssn3^{AS} with 3-MB-PP1 compared to WT with 3-MB-PP1 and of Ssn3^{AS} with 3-MB-PP1 compared to with the DMSO control. The heat map shows Log2-transformed counts per million for expressed transcripts.

977 peptides with decreased phosphorylation >2 fold upon Ssn3^{AS} inhibition with 3-MB-PP1

↓

218 proteins with 2 or more peptides with decreased phosphorylation >2 fold with Ssn3 inhibition

↓

<u>41 putative Ssn3 targets with known or predicted nuclear localization</u>

Blm3, Bre1, Bur1, Cdc54, Cet1, Crz1, Cta8, Dbp3, Def1, Eaf7, Eed1, Fip1, Flo8, Isw2, Kel1, Krr1, Leu3, Med4, Mob2, Msn4, Not5, Pwp2, Rrp36, Rtg1, Rtg3, Set1, Set3, Smt3, Snf2, Stb3, Taf12, Zds1, C1_03360W(Chd1), C1_13880C(Zms1), C2_08720W, C2_09880C, C2_05640W(Bas1), C3_03670W(Hda2), C6_01590W, CR_02510W, CR_04110W(Naf1)

Figure 4. Overview of proteins for which two phosphopeptides were lower by >2 fold upon inhibition of Ssn3. Focusing on peptides that were significantly lower in Ssn3^{AS} treated with 3-MB-PP1 relative to control cultures ($p<0.05$ FDR-corrected), we found 977 peptides that were 2-fold lower upon 3-MB-PP1 inhibition of *ssn3^{AS}* relative to changes in SC5314 WT. Two hundred and eighteen proteins had two more peptides that met these criteria, forty of which were predicted to have nuclear localization. Med4 is a validated *C. albicans* Ssn3 target. If an alias is available for an unnamed gene, it is shown in parentheses.

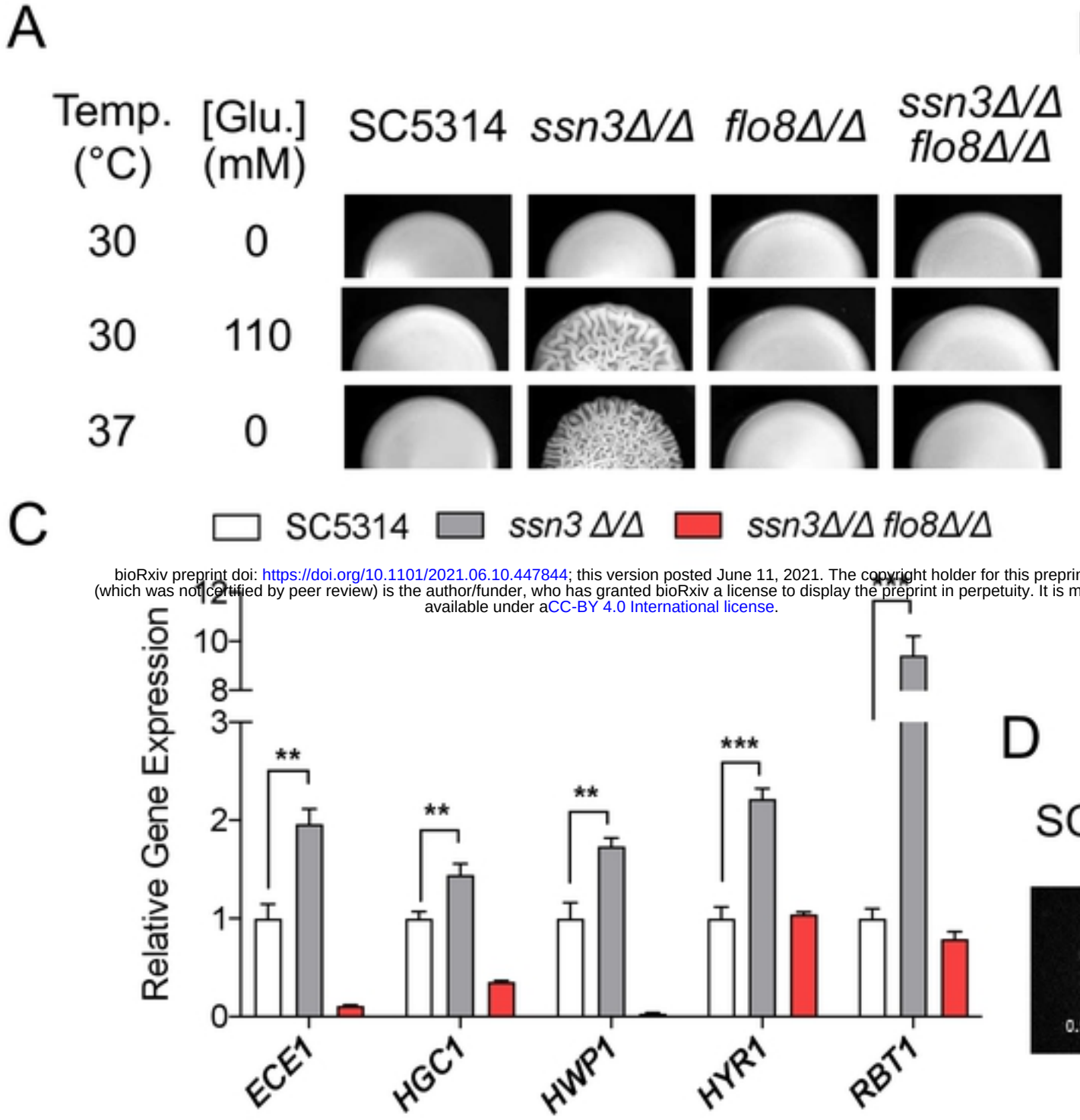

Figure 5. *SSN3* repression of filamentation is *FLO8* dependent. A. Colony morphology of a wild type *C. albicans* strain (SC5314), *ssn3Δ/Δ*, *flo8Δ/Δ* and *ssn3Δ/Δ flo8Δ/Δ* strains grown on YNBA agar medium alone or supplemented with 110 mM glucose at 30°C or on YNBA at 37°C. B. Cell morphology of strains tested in (A) after cells were grown in $YNBN_{2.5}AG_{11}$ at 30ºC for 3 hours. C. NanoString analysis of indicated hypha-specific genes over-expression in the SC5314 wild type, and *ssn3Δ/Δ, and ssn3Δ/Δflo8Δ/Δ* mutants. RNA was extracted from cells grown as indicated for (B) but for 75 minutes. Gene expression was represented by mean and standard deviation after normalization to Nanostring positive controls, and *TEF1* and *ACT1* reference transcripts; expression of each gene in the wild type strain (SC5314) was set to '1'; **, $p<0.01$ and ***,$p<0.001$. D. The embedded colonies of the same set of strains shown in (A) grown in YPS at 25°C.

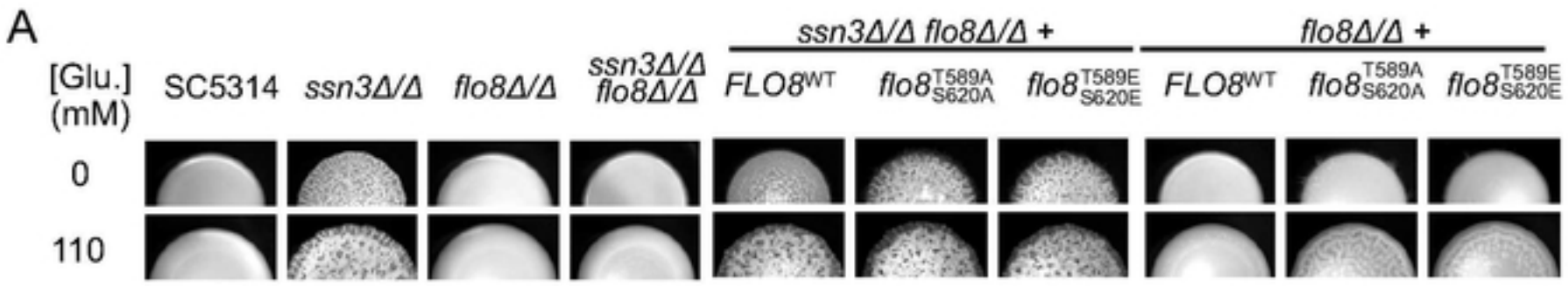

Figure 6. Residues identified as phosphorylation sites influence Flo8 function. A. SC5314 wild type, *ssn3Δ/Δ*, *flo8*Δ/Δ and *ssn3*Δ/Δ*flo8*Δ/Δ strains were imaged after growth as colonies on YNBA or YNBA+110 mM glucose at 37˚C. *flo8*Δ/Δ and *ssn3*Δ/Δ*flo8*Δ/Δ expressing C-terminally 3XHA tagged $Flo8^{WT}$, $Flo8^{T589A/S620A}$ or $Flo8^{T589E/S620E}$ were also included. B. Cell morphology of SC5314, *flo8*Δ/Δ, and *flo8*Δ/Δ expressing 3XHA-tagged $Flo8^{WT}$, $Flo8^{T589A,S620A}$ or $Flo8^{T589E,S620E}$ after growth in $YNBN_{2.5}AG_{11}$ at 30°C for 3h. C. Gene expression in *flo8*Δ/Δ expressing 3XHA-tagged $Flo8^{WT}$ or $Flo8^{T589A/S620A}$ relative to *flo8*Δ/Δ after growth in YNBNAG for ~2h. Data show the mean and standard deviation from measurement on triplicate RNA samples. Gene expression in *flo8* mutant (not shown) was set to '1'. P-values (t-tests) were directly denoted or indicated by '*' ($p<0.05$), '**'($p<0.01$) or '***' ($p<0.001$) to show statistically significant differences. D. Immunoblotting analysis with an α-HA antibody showing levels and gel mobility of native Flo8 with the C-terminal 3X-HA tag or variants with T589A,S620A or T589E,S620E substitutions; proteins were expressed in either *flo8*Δ/Δ or *ssn3*Δ/Δ *flo8*Δ/Δ backgrounds and were grown in YNBAG at 30˚C to mid-log phase. E. Flo8-HA levels in strains with full Ssn3 activity, SC5314 ($Ssn3^{WT}$) and $ssn3^{AS}$, or without Ssn3 activity (*ssn3*Δ/Δ or $ssn3^{KD}$).

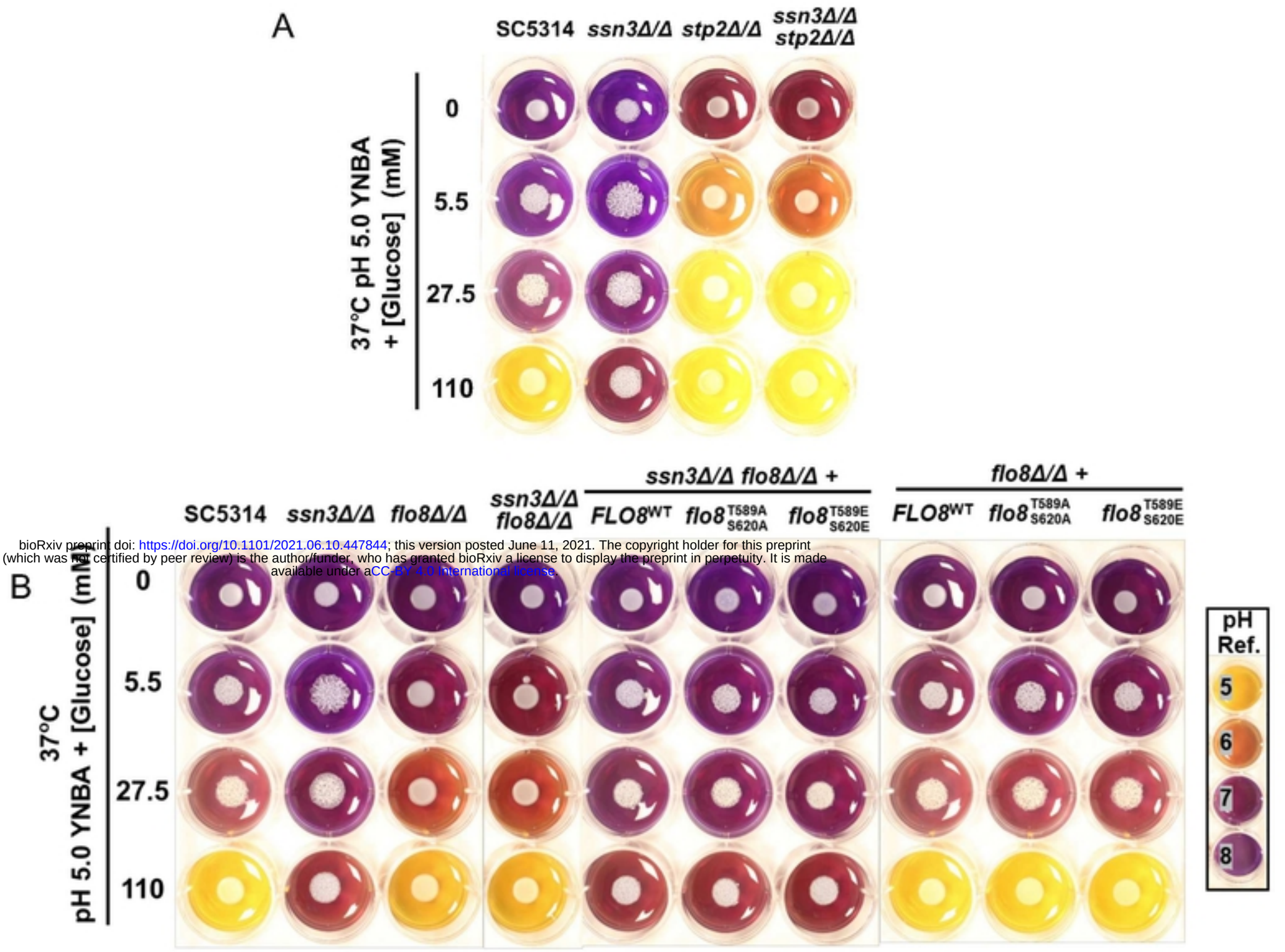

Figure 7. Medium alkalinization is affected by Ssn3 and Stp2. A. Comparison of medium pH by growth of SC5314, *ssn3Δ/Δ*, *stp2Δ/Δ* and *ssn3Δ/Δ stp2Δ/Δ* strains at 37°C. B. *ssn3* hyperalkalinization phenotype is dependent on *FLO8* at 37°C. SC5314, *ssn3Δ/Δ*, *flo8Δ/Δ* and *ssn3Δ/Δflo8Δ/Δ* alone or expressing C-terminally 3XHA tagged Flo8^{WT}, Flo8$^{T589A/S620A}$ or Flo8$^{T589E/S620E}$. Medium pH was assessed on YNBA with increasing concentrations of glucose and bromocresol purple as a pH indicator.